Robust spatial navigation in a robot inspired by chemotaxis in *C. elegans*

T. M. Morse, T. C. Ferrée and S. R. Lockery
Institute of Neuroscience
University of Oregon
Eugene, OR 97403-1254

February 10, 2001

Abstract

We report on the design and implementation of an autonomous robot that performs phototaxis under the control of a simulated neural network. The mechanical configuration of the robot and its neural network controller are patterned after those believed to produce chemotaxis in the nematode *Caenorhabditis elegans*. The network is first optimized to produce phototaxis in a simulated, nematode-like robot, and is then tested on a real robot. We find that both the simulated and real robot perform reliably, making nearly identical trajectories for similar environments and similar starting conditions. Furthermore, their performance is robust to significant perturbations of the robot's locomotion parameters. Finally, we discuss the implicit computational rule this network uses to control phototaxis. This makes the results intuitive, and improves our intuition about control of taxis behavior in two dimensions.

Adaptive Behavior 6: 391-408. MIT Press (1998).
Special Issue on Biologically Inspired Models of Spatial Navigation.

1 Introduction

An autonomous robot must be able to orient itself to its environment. One approach to designing orientation controllers takes inspiration from biology, since even the simplest animals display impressive control capabilities (Berg and Brown, 1972). In the animal world, survival depends critically upon the ability to orient in space. Orientation behavior is central to seeking out hospitable environments, locating food, and finding a mate. Many species, therefore, have evolved mechanisms for detecting and orienting to a wide range of stimulus fields (Bell, 1991; Schöne, 1984). Moreover, the central importance of orientation behavior suggests it should be robust to unexpected perturbations of the stimulus field, the animal's internal state, or the orientation mechanism itself. Evidence from studies of animal orientation indicate that it is, indeed, quite robust (Gould, 1986; Schmidt-Koenig and Schlichte, 1972). Thus, understanding how animals orient is likely to provide insights into robust control mechanisms for spatial behavior which can be applied to control orientation behavior in autonomous robots.

The tiny soil nematode *Caenorhabditis elegans* is an excellent experimental system in which to study orientation behavior. It locates food by chemotaxis, the ability to orient in response to gradients of chemical concentration. *C. elegans* chemotaxis behavior is remarkably robust, since the nematodes can orient to gradients that vary in intensity by four orders of magnitude (Ward, 1973). Moreover, chemotaxis is resistant to a variety of genetically induced perturbations of its systems for chemical detection (Bargmann *et al.*, 1993; Coburn and Bargmann, 1996; Culotti and Russell, 1978) and locomotion (Ward, 1973). *C. elegans* is also advantageous because it has a simple nervous system of only 302 neurons, which has made possible a complete description of the morphology and synaptic connectivity of all its neurons (White *et al.*, 1986). This information has been combined with genetic analysis and neuronal ablations to determine which neurons are required for many *C. elegans* behaviors (Bargmann, 1993), including chemotaxis (C. Bargmann, pers. comm.). Thus, an analysis of chemotaxis in *C. elegans* is likely to provide insights into robust, neural-network control mechanisms for spatial orientation behavior.

In this paper, we analyze the performance of a neural network used to control orientation in an autonomous robot. The architecture and dynamics of the network are based on the prominent features of the biological network believed to control chemotaxis in *C. elegans*. Synaptic connection strengths are optimized to produce chemotaxis-like orientation behavior in a simulated, nematode-like robot. Orientation in the simulated robot is demonstrated to be robust to significant perturbations of its locomotion parameters. The same network is then implemented in an actual, nematode-like robot. We find that the actual robot performs reliably, producing movements nearly identical to those of the simulated robot. We also find that control of the robot by this network is robust to perturbations of the robot's locomotion

parameters. Finally, using a recently derived method for rule extraction in neural networks (Ferrée and Lockery, 1997), we discuss the computational algorithm which the network implicitly uses to control orientation. This makes intuitive the results obtained for the robot, and improves our intuition about spatial navigation in two dimensions.

2 The control problem

Chemotaxis in *C. elegans* is most commonly studied by establishing a two-dimensional gradient of chemical concentration, approximately gaussian in shape, at the center of a round Petri plate (Ward, 1973). Nematodes are released at some distance from the center of the gradient and allowed to explore the plate. After initial wandering movements, they orient almost directly up the gradient, then dwell at its center (Fig. 1). Thus, chemotaxis in *C. elegans* is not a biased random walk, as in bacteria (Berg and Brown, 1972), but reflects true orientation to the chemical gradient.

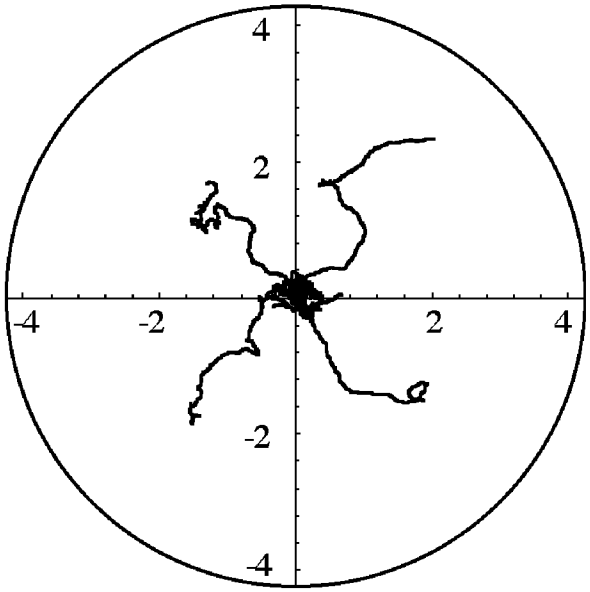

Figure 1: Chemotaxis behavior in *C. elegans*. Each line represents the track of one of four worms responding to a two-dimensional, gaussian-shaped gradient of NH_4Cl, centered at the point $(0, 0)$. Dimensions are in centimeters.

C. elegans chemotaxis presents a well-posed control problem for modeling and robotics. The control problem is defined by three physical constraints.

1. The animal detects the chemical environment at a single point in space. *C. elegans* has a pair of chemosensory organs, called amphids, located on the left and right sides of its head. During ordinary locomotion on a flat surface, however, the animal moves on its right or left side, propelling itself with dorsal-ventral contractions. Thus the amphids are oriented perpendicular to the gradient, and they are exposed to essentially the same chemical concentration. This means the nematode senses the concentration at a single point in space. To gain information about the chemical gradient, therefore, the nematode must make temporal comparisons of the local concentration as it moves through its environment.

2. Observation of chemotaxing nematodes reveals that the direction of movement is determined by the angle of the head with respect to the body. The angle of the head is controlled by two sets of head and neck muscles, one on each side of the body (Fig. 2a). Each set can be considered a single effector, however, since the muscles comprising a set are close together and appear to act in unison.

3. Behavioral experiments indicate that the instantaneous speed of *C. elegans* is nearly constant during chemotaxis (Pierce and Lockery, unpublished). Since movement in two dimensions is fully described by speed and direction, this leaves direction of locomotion as the most likely control variable.

In light of these constraints, the control problem is to find a mapping between the sensory input at the nose and the activity of the pair of effectors controlling the angle of the head such that the animal (or robot) orients up a gradient and dwells at its peak.

3 Equations of motion for nematode-like chemotaxis

The solution to the nematode control problem depends on the equations of motion chosen to represent nematode locomotion. Figure 2a shows the idealized nematode body from which these equations were derived. A nematode generates locomotory thrust by making snake-like sinusoidal movements of its body. For the purpose of the model, however, the body is represented as a lumped force-generating mechanism. Chemical concentration is sensed at the point (x, y). The bold arrow indicates the velocity vector $\vec{v}$, with associated speed v and direction θ. Its components can be written

$$\begin{aligned} \frac{dx}{dt} &= v \cos\theta \\ \frac{dy}{dt} &= v \sin\theta \end{aligned} \tag{1}$$

where v is constant and θ is a function of time.

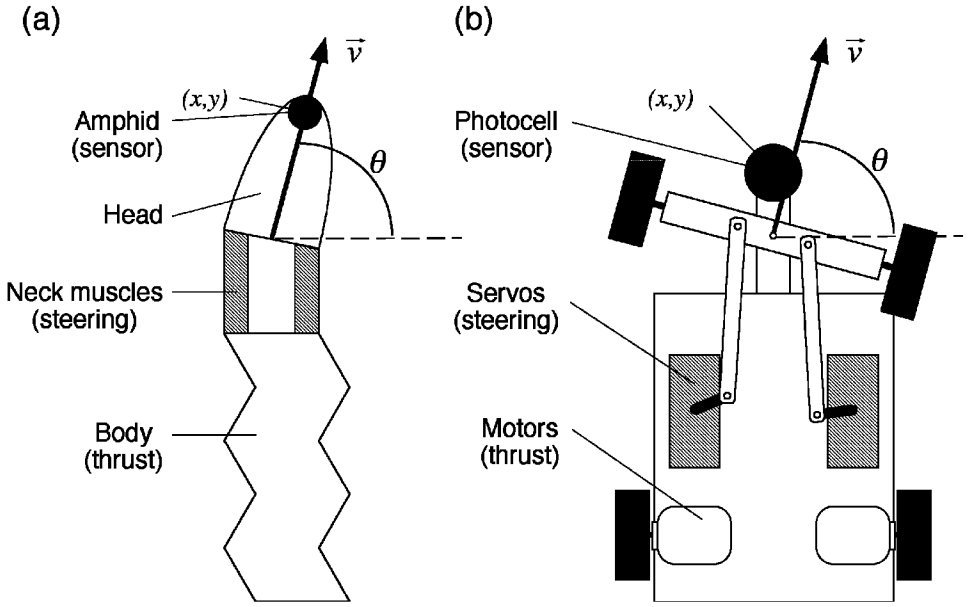

Figure 2: Schematic representations of (a) an idealized nematode, and (b) the nematode-like robot. The nematode has a head, flexible neck, and body. Chemical concentration is detected at the point (x, y) by a pair of sensory organs (amphids), one of which is visible in the diagram. The direction of movement θ is controlled by a pair of neck muscles that set the angle of the head. The nematode moves at constant speed v in response to thrust provided by undulatory motion of the body. The robot is analogous to the nematode. The amphids are represented by a photocell that detects light intensity at the point (x, y). The neck muscles are represented by servos that control the angle of the front wheels. Thrust produced by the nematode is represented by the force produced by a pair of motors that drive the robot at constant speed v.

We assumed the nematode moves without slipping. Thus, the rate of turning $d\theta/dt$ is determined by the angle of the head (Ferrée, *et al.*, 1997). In the model, this angle is determined geometrically by the relative length of dorsal and ventral neck muscles which, in turn, are determined by the voltages of the corresponding motorneurons. Assuming that the body posture responds instantly to neural commands, and the length of an individual neck muscle is proportional to the voltage of its corresponding motor neuron, we have

$$\frac{d\theta}{dt} = \gamma \left(V_{\mathrm{D}} - V_{\mathrm{V}} \right) \tag{2}$$

where V_{D} and V_{V} are dorsal (D) and ventral (V) motor neuron voltages. The constant parameter γ is chosen so the model produces tracks with behaviorally appropriate turning

rates. Note that if V_D and V_V are constant, then $d\theta/dt$ is constant, and θ increases linearly with t. Equations (1) then make a circle with radius $R = v/(d\theta/dt)$. A special case is when $V_D = V_V$, so that $d\theta/dt = 0$ and θ is constant. Equations (1) then make a straight line.

4 The nematode-robot analogy

In previous work, we found that model neural networks can be optimized to solve the chemotaxis control problem for a simulated nematode in a simulated gradient (Ferrée *et al.*, 1997; Ferrée and Lockery, 1997). This was done by numerically optimizing the synaptic connection strengths in idealized chemotaxis networks. It is often the case, however, that a control mechanism that performs well in simulations does not perform well in real-world applications. This is because the real world presents unforeseen complications such as noise, environmental variability, and imperfections in the device to be controlled. To assess the reliability of neural network solutions in a real-world application, therefore, we asked whether a network optimized to control a simulated nematode-like robot could control an actual nematode-like robot.

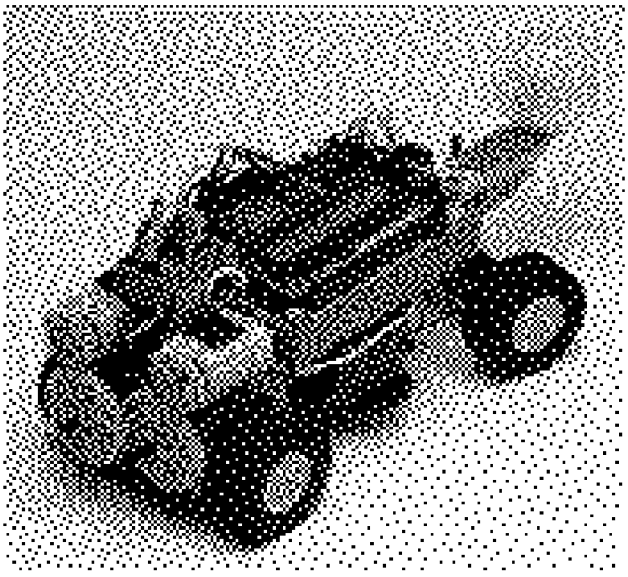

Figure 3: Photograph of the nematode-like robot showing the on-board circuitry, drive gears, and servos. The photocell is housed in the translucent dome at the front. The robot is 28 cm long.

The robot was a simple, four-wheeled cart (Figs. 2b, 3). Although a variety of snake-like robots are available (Hirose, 1993; Worst and Linnemann, 1996), the cart was sufficient to embody the three essential features of the control problem.

1. The cart was equipped with a single sensor, to maintain the analogy with *C. elegans*, in which the chemical environment is sensed at a single point.

2. The angle of the front axle relative to the body, and hence the rate of turning $d\theta/dt$, was controlled by a pair of effectors on either side of the robot, corresponding to the head and neck muscles on either side of the nematode body.

3. The cart was driven by a pair of motors operating at constant speed v.

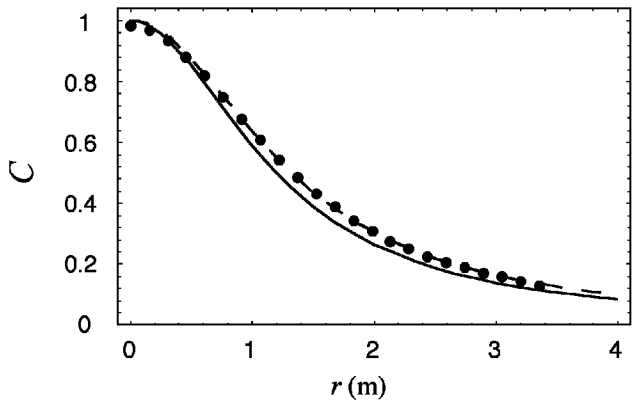

Figure 4: Light environment used for real and simulated robots. The solid line shows the normalized light intensity C used during optimization of the simulated robot; the light is a point source 120 cm above the floor. The filled circles show the normalized light intensity $C_{\rm meas}$ computed from the measured photocell output $P_{\rm raw}$ in the actual robot testing environment. The dashed line shows the best fit of equation (3) to the data, yielding an effective light height of 132 cm.

Because it is difficult to make and detect chemical gradients on a scale big enough for the robot, we substituted a gradient of light intensity for the chemical gradient. Thus, we used phototaxis as an analogy to chemotaxis and substituted a photocell for the chemosensory organs of the actual nematode. A 100W light bulb was hung approximately 120 cm above the floor. On this distance scale, the bulb acts like a point source, and the light intensity forms a stimulus field which can be fit by

$$C(x,y) = \frac{h^2}{x^2 + y^2 + h^2} \tag{3}$$

where h is the distance between the floor and the bulb. The intensity C has been normalized, so that $C = 1$ at the origin $x = y = 0$. The solid curve in Fig. 4 shows C as a function of r, where $r \equiv \sqrt{x^2 + y^2}$.

5 Biological neural network for chemotaxis in *C. elegans*

Laser ablation experiments have identified approximately 40 neurons which are important for chemotaxis (Bargmann and Horvitz, 1991; Bargmann *et al.*, 1993; C. Bargmann, pers. comm.) including chemosensory neurons, interneurons, and motor neurons. In combination with the anatomical data on the synaptic connectivity of the *C. elegans* nervous system (White *et al.*, 1986), these experiments indicate that the chemotaxis network is highly interconnected, with numerous feedforward and feedback connections.

Biophysical analysis of neurons in the head ganglia of *C. elegans*, where the chemotaxis circuit lies (C. Bargmann, pers. comm.), indicates that neurons in the chemotaxis circuit are likely to be functionally isopotential (Goodman *et al.*, 1998; Goodman and Lockery, unpublished). Thus (to a first approximation) each neuron can be represented as a single isopotential compartment with voltage as its state variable. This has two main implications which are relevant for robotics. First, since each neuron is described by a single differential equation, the network equations are not particularly stiff and can be numerically integrated on modest machines in a reasonable amount of time. Second, the computational algorithms which are implicitly implemented by such a network are analog in nature, and cannot rely on complex coding of spike arrival times, as is likely the case in many other systems (Rieke *et al.*, 1997). This simplifies the prospect of implementing such a network in analog VLSI, an important direction for future work.

6 Model neural network for phototaxis in the robot

To control the robot, we used a small neural network which embodies the essential features of the biological network described above. The network had a single sensory neuron, three interneurons, and a pair of motorneurons which innervate dorsal and ventral muscles (Fig. 5 "effectors"). The voltage V_i of each neuron obeys

$$\tau_i \frac{dV_i}{dt} = -V_i + \sum_{j=1}^{N} w_{ij} \, (V_j - \overline{V}_j) + \kappa \delta_{i1} C(t) \tag{4}$$

where τ_i is its membrane time constant, w_{ij} represents the strength of the synaptic connection from neuron j to neuron i, and $\overline{V}_j$ is the presynaptic voltage at which there is no synaptic transmission. The last term represents input to the sensory neuron, obtained by evaluating (3) at the instantaneous position of the nose:

$$C(t) \equiv C(x(t), y(t)) \tag{5}$$

The parameter κ in (4) is a constant with units of volts.

The neural network defined by (4) is linear. It contains no voltage-dependent conductances and the postsynaptic effect of a synapse is a linear function of presynaptic voltage V_j. This represents a considerable simplification because the biological chemotaxis network is likely to contain voltage-dependent conductances and non-linear synaptic functions (Davis and Stretton 1989; Goodman *et al.*, 1998). The linear case is a good starting point, however, because previous work has shown such networks to be sufficient to control chemotaxis in simulated nematodes and, moreover, linear networks have the significant advantage of allowing analytic solutions which reveal their implicit control algorithms (Ferrée and Lockery, 1997). We expect that analysis of the linear case will help us understand the nonlinear case in the future.

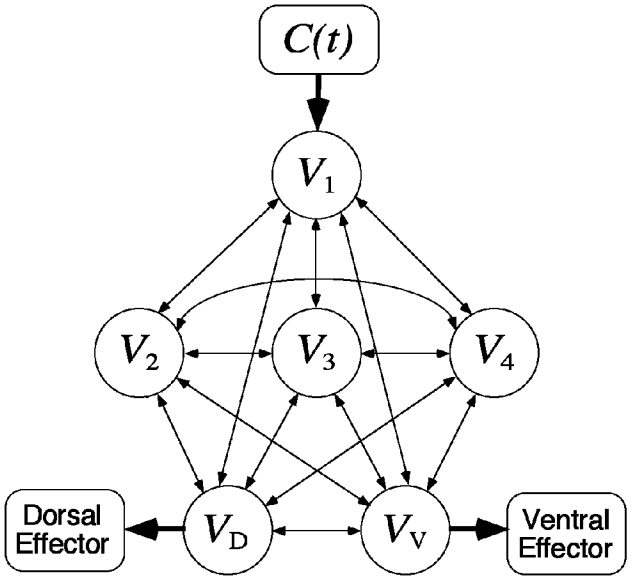

Figure 5: The neural network model. Each neuron is represented as a single isopotential compartment, with voltage V_i as its state variable. The network has a single sensory neuron V_1, three interneurons ($V_2 - V_4$) and a pair of motor neurons (V_D and V_V). The sensory neuron receives continuous input $C(t)$, and the motor neurons send output to dorsal and ventral effectors. Connections are represented by double-headed arrows, indicating that each neuron is presynaptic to all other neurons in the network.

7 Optimization of the model network

Parameters in the model neural network were optimized to produce phototaxis in a simulated, nematode-like robot. Ideally, one would like to optimize the network while it is controlling the real robot, but this is impractical, because the optimization procedure requires many

iterations, and the robot runs too slowly to make this feasible. Instead, the network was optimized to control a computer simulation of the real robot. The optimization procedure was based on quantifying the network's ability to control phototaxis efficiently for a variety of initial conditions. Each parameter set $\Gamma \equiv \{\tau_i, w_{ij}, \overline{V}_j, \kappa\}$ can be thought of as a different candidate network, allowed to control the simulated robot as it explores its environment. Each set Γ was assigned a fitness F for phototaxis

$$F(\Gamma) = \left\langle \frac{1}{T} \int_0^T C(t)\, dt \right\rangle_{\{x_0, y_0, \theta_0\}} \tag{6}$$

where T is the simulation time, and $C(t)$ is defined in (5). The average was taken over a predetermined set of initial positions and angles. Initial voltages were always chosen to correspond to the equilibrium state of the network with no input.[1] Both the simulated and real robots explored their environment for $T = 3$ minutes.

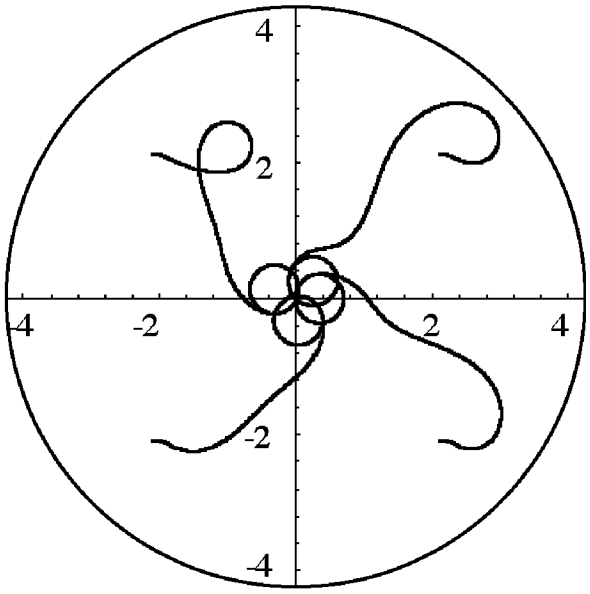

Figure 6: Phototaxis behavior of the simulated robot. Each line shows the robot's trajectory in the gradient shown by the solid line in Fig. 4. Dimensions are in meters.

The network was optimized for phototaxis by searching over the space of parameters Γ to maximize $F(\Gamma)$. The linearity of (4) enabled us to restrict the search to networks which were stable, i.e., networks in which the voltages V_i remain finite. This was done by requiring that the characteristic eigenvalues of (4) all have negative real parts (Ferrée and Lockery,

[1]These can be obtained from (4) by setting $C = 0$ and $dV_i/dt = 0$, and solving for V_i.

1997). This decreased optimization time considerably, since equations (1), (2) and (4) were numerically integrated only if this condition was satisfied. We then used a simple simulated annealing algorithm (Masters, 1995) to find an optimal set Γ. Many such sets were found which perform phototaxis reliably, but a single typical one was chosen for further study.

Figure 6 shows the output of the network defined by this set, for $v = 6$ cm/sec and $h = 120$ cm. For each initial condition, the simulated robot oriented up the gradient and dwelled near its peak. Dwelling was achieved by turning constantly at the minimum turning radius ($R_{\min} \simeq 34$ cm). A minimum radius was imposed on the simulated robot to make it consistent with the mechanical limit on turning radius in the real robot.

8 Linking the model network and the robot

The robot was based upon a commercially available robotic interface (Handy Board[2]). The board contains a 2 MHz 68HC11 microprocessor and is equipped with analog to digital converters for the photocell and servos. Because the board has only 32k of static RAM and does not have a floating point processor, simulating the model network on board was not feasible. Instead, the network was simulated on a Gateway 2000 personal computer (PC) with a 486 MHz processor, which communicated with the interface board via a tether. The PC used a forward Euler algorithm ($\Delta t = 100$ ms) to update the voltages of the network according to equation (4).

The photocell output, P_{raw}, was normalized using

$$C_{\text{meas}} = \frac{P_{\text{raw}} - P_{\text{dark}}}{P_{\text{bright}} - P_{\text{dark}}} \tag{7}$$

where P_{bright} and P_{dark} are constants. When running the robot, C_{meas} was used for $C(t)$ in (4).

The front axle of the robot was controlled by a pair of servos (Fig. 2b). Each servo received an input S, given by

$$S = \frac{k_{\text{steer}}}{v} \frac{d\theta}{dt} + 100 \tag{8}$$

where k_{steer} is a constant, and $d\theta/dt$ is the desired rate of turning. When running the robot, $d\theta/dt$ was computed from the motor neuron voltages using equation (2).

[2]See http://el.www.media.mit.edu/groups/el/projects/handy-board/.

9 Robot performance

9.1 Phototaxis behavior

After optimization, the simulated robot exhibited reliable phototaxis. From a range of initial positions and starting angles, it oriented up the gradient and dwelled at its peak (Fig. 6) much like the real nematode (Fig. 1). Phototaxis can also be represented by plotting the light intensity sensed by the robot as function of time. Figure 7 shows this plot for the simulated robot track starting in the lower right quadrant of Fig. 6. The stimulus field used in the simulation that generated this plot is described by (3), for $h = 132$ cm, corresponding to the effective light height perceived by the robot (see Fig. 4). Light intensity increased smoothly, then oscillated as the robot orbited near the peak of the gradient. When the real robot was run from the same initial condition, a very similar trajectory was observed (Fig. 7). Similar results were obtained from all four initial conditions shown in Fig. 6, indicating that the real robot exhibited reliable phototaxis.

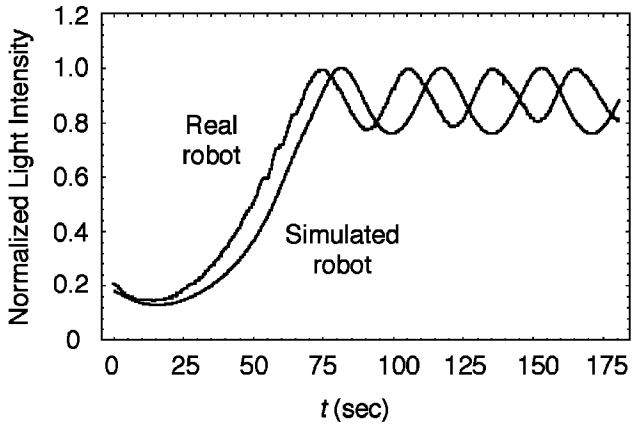

Figure 7: Sensory representation of the phototaxis behavior of the real and simulated robots. Normalized stimulus intensity $C(t)$ is plotted versus elapsed time t as the robots explored their environments. Both robots moved smoothly to a location near the peak of the stimulus field (intensity = 1) and dwelled there.

9.2 Robustness

To study the robustness of phototaxis control by the neural network, we measured the fitness of the simulated and real robots as functions of two biologically plausible perturbations of its locomotion: change in instantaneous speed, and addition of a constant turning bias. In all perturbation experiments the robots were started a distance $r_0 = 2\sqrt{2}$ meters from the

origin. Fitness was computed as defined in (6) and averaged over the 4 initial positions (x_0, y_0) and starting angles θ_0. For the real robot, fitness was computed using the actual light intensity C_{meas}, defined in (7).

Speed. The performance of the simulated and the real robots was robust to changes in speed. This is indicated by the pronounced plateau in the plot of fitness versus speed shown in Fig. 8a for both robots. For the simulated robot, fitness has a plateau ranging from $v = 6$ cm/sec to $v = 16$ cm/sec. For $v < 6$ cm/sec the fitness dropped abruptly, and for $v < 3$ cm/sec the fitness was approximately constant. This minimum was reached abruptly because at low speeds the robot made a circular path near its starting point, never orienting toward the light source. At high speeds the fitness dropped more gradually, falling by $1/e$ at approximately $v = 21$ cm/sec. This reduction occurred because the robot made wide arcs around the light, never reaching the origin at the highest speeds. Although the extent of the plateau for the real robot was nearly the same as for the simulated robot, average fitness for the real robot was consistently higher. This may be due to non-ideal behavior of the photocell. Taken together, these results suggest that a robot using this network controller and run at speeds near 11 cm/sec should function reliably despite significant ($\pm 45\%$) variations in speed, such as might occur due to differences in terrain, reduction of power, etc.

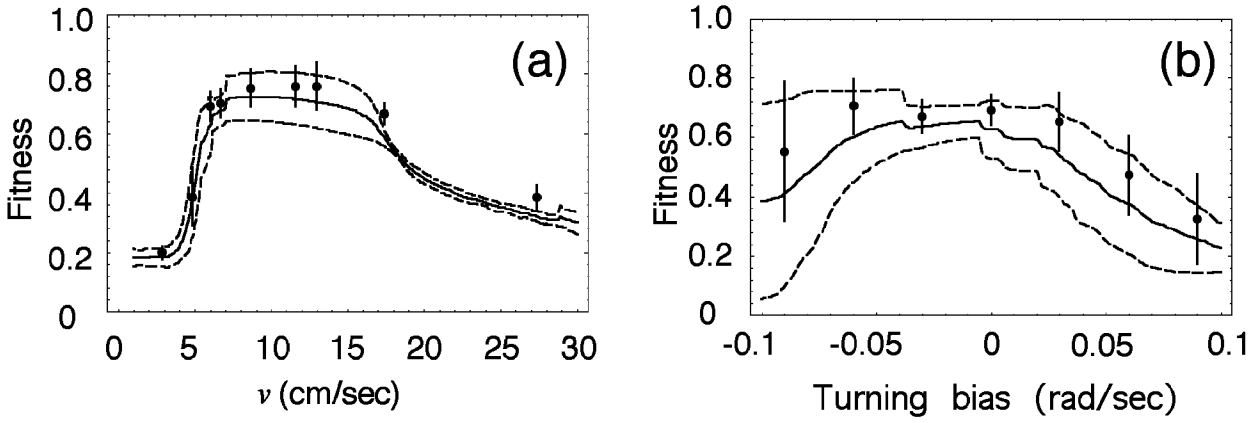

Figure 8: Tests of robustness in the performance of the simulated and real robots. (a) Fitness as a function of speed. The solid line shows the fitness of the simulated robot averaged over the 4 initial conditions shown in Fig. 6. The dashed lines are $\pm$ one standard deviation about the mean. The filled circles show the fitness of the real robot averaged over the same 4 initial conditions. The vertical bars are $\pm$ one standard deviation about the mean. (b) Fitness as a function of turning bias. Symbols are the same as in (a).

Turning bias. The performance of the simulated and the real robots was also robust to addition of a constant turning bias. This was achieved by adding a constant to equation (2).

The fitness of the simulated robot changed relatively little over the range zero to approximately -0.05 rad/sec, and fell off nearly symmetrically about the center of this range. Fitness fell by $1/e$ of its maximum value at biases of approximately -0.085 and +0.05, corresponding to 48% and 28% of the real robot's maximum turning rate, respectively. Similar results were obtained for the real robot (although, again, its fitness was consistently higher than that of the simulated robot). In real-world applications, therefore, a robot using this controller should function reliably despite significant misalignment or wear in the steering mechanism, mismatched servos, etc.

10 Discussion

To interpret the results just presented, we apply a method of rule extraction recently derived for linear recurrent networks (Ferrée and Lockery, 1997). Since equations (4) are linear in voltage, they can be solved analytically and combined with (2) to yield an analytic expression for the rate of turning at time t:

$$\frac{d\theta}{dt} = \Omega_{\text{network}} + \int_0^T k(t-t')C(t')\ dt' \tag{9}$$

where Ω_{network} is a constant turning bias. This bias is intrinsic to the network in that it arises from the constant parameters $\bar{V}_j$ in (4), and should not be confused with the mechanical bias introduced in Section 9. The integral is a convolution of the input history $C(t')$ with a kernel $k(t-t')$, which completely characterizes the response of the network. This solution can be manipulated to yield an approximate expression for $d\theta/dt$ in terms the instantaneous input $C(t)$ and its time derivatives:

$$\frac{d\theta}{dt} \simeq\ 0.0493 + 0.5819\ C(t) - 19.14\ \frac{dC}{dt} + ... \tag{10}$$

The constant coefficients were derived from the kernel, and depend on all of the network parameters Γ. Since C has no explicit time dependence, its time derivative can be written

$$\frac{dC}{dt} = \vec{v} \cdot \vec{\nabla} C \tag{11}$$

where the velocity vector $\vec{v}$ is defined as in (1). Keeping terms only through first order in d/dt, equation (10) can be integrated with equations (1) to generate simulated robot tracks which are nearly identical to those shown in Fig. 6 (Ferrée and Lockery, 1997).

Equation (10) can be used to understand the computational rule which the network implicitly uses to control phototaxis. The first term is a constant turning bias Ω_{network} such that if $C = 0$, then the robot makes a circle with radius $R = v/\Omega_{\text{network}} \simeq 122$ cm. The second term (proportional to C) implies that if C is constant, then R decreases as a function

of C. These two terms alone are not sufficient to produce taxis behavior, however. The third term (proportional to dC/dt) has opposite sign, and is essential for taxis behavior in the following way. When the robot is moving away from the light, $dC/dt < 0$, and the net turning rate is increased; this results in a reorientation of the robot toward the light. When the robot is moving toward the light, $dC/dt > 0$, and the net turning rate is decreased; this results in the robot making progress up the gradient. Thus phototaxis control by this network arises from a competition between the derivative term dC/dt and the first two terms in (10). This result is intuitive, since taxis is defined as oriented movement in a stimulus gradient, and (11) shows that dC/dt has a simple relation to the gradient $\vec{\nabla}C$.

Equation (10) can also be used to understand the dependence of the robot's fitness on speed, shown in Fig. 8a. From (11) we see that the derivative term in (10) is proportional to the speed v, therefore the speed of the robot modulates the degree to which the gradient affects the rate of turning. At low v, the network simply can not respond to the gradient, and the robot moves in a nearly circular path near its starting point. Thus the fitness decreases abruptly. In contrast, at very high v, the derivative term in (10) dominates the other two terms. This results in circular paths around the light source, since paths of this sort satisfy $d\theta/dt \simeq 0$ and $dC/dt \simeq 0$ simultaneously.

Finally, equation (10) can be used to explain the dependence of the robot's fitness on a mechanical turning bias (Fig. 8b). The mechanical bias and the intrinsic network bias Ω_{network} add. When the net turning bias is large, it dominates the equation, leading to circular arcs near the robot's starting position. The fact that the intrinsic bias in equation (10) is positive explains the leftward shift of the fitness curve in Fig. 8b.

11 Conclusions

Our results show that a neural network inspired by the neural circuitry for chemotaxis in *C. elegans* can be optimized to produce chemotaxis-like orientation behavior in an autonomous robot. Orientation was robust to perturbations of speed and turning bias as large as 45%. Robustness was an emergent property of the system, since the simulated robot ran at constant speed and with no turning bias during optimization. This suggests that a *C. elegans*-like neural network for orientation is inherently robust. It is likely, however, that robustness to perturbations in speed and bias could be improved by including these perturbations in the optimization procedure.

Acknowledgments

The authors thank B. Marcotte, J. T. Pierce and C. J. Roehrig for valuable discussions.

This work was supported by NIMH MH11373, NIMH MH51383, NSF IBN 9458102, ONR N00014-94-1-0642, the Sloan Foundation, and the Searle Scholars Program.

References

Bargmann, C. I. (1993). Genetic and cellular analysis of behavior in *C. elegans*. *Annu. Rev. Neurosci.* **16**: 47-71.

Bargmann, C. I., E. Hartwieg and H. R. Horvitz (1993). Odorant-selective genes and neurons mediate olfaction in *C. elegans*. *Cell* **74**: 515-527.

Bargmann, C. I. and H. R. Horvitz (1991). Chemosensory neurons with overlapping functions direct chemotaxis to multiple chemicals in *C. elegans*. *Neuron* **7**: 729-742.

Beer, R. D., R. E. Ritzmann and T. McKenna (1993). *Biological neural networks in invertebrate neuroethology and robotics*. Academic Press, Inc.

Bell, W. J. (1991). *Searching behavior: The behavioural ecology of finding resources*. Chapman and Hall.

Berg, H. C. and D. A. Brown (1972). Chemotaxis in *Escherichia coli* analyzed by three-dimensional tracking. *Nature* **239**: 500-504.

Coburn, C. M. and C. I. Bargmann (1996). A putative cyclic nucleotide-gated channel is required for sensory development and function in *C. elegans*. *Neuron* **17**: 695-706.

Davis, R. E. and A. O. W. Stretton (1989). Signaling properties of *Ascaris* motorneurons: Graded active responses, graded synaptic transmission, and tonic transmitter release. *J. Neurosci.* **9**: 415-425.

Dunn, G. A. (1990). Conceptual problems with kinesis and taxis. In *Biology of the chemotactic response*, J. P. Armitage and J. M. Lackie (eds.). Cambridge University Press.

Ferrée, T. C., B. A. Marcotte and S. R. Lockery (1997). Neural network models of chemotaxis in the nematode *Caenorhabditis elegans*. In *Advances in Neural Information Processing Systems* **9**:55-61. MIT Press.

Ferrée, T. C. and S. R. Lockery (1997). Extracting computational rules from linear recurrent networks. Submitted to *Neural Computation.*

Goodman, M. B., D. H. Hall, L. Avery and S. R. Lockery (1998). Intrinsic electrical properties of *C. elegans* neurons investigated by whole-cell patch-clamp recording. *Submitted.*

Gould, J. L. (1986). The local map of honeybees: Do insects have cognitive maps? *Science* **232**: 861-863.

Hirose, S. (1993). *Biologically inspired robots: Snake-like locomotors and manipulators.* Oxford University Press.

Masters, T. (1995). *Advanced algorithms for neural networks: A C++ sourcebook.* John Wiley & Sons, Inc.

Reike, F., D. Warland, R. de Ruyter van Steveninck and W. Bialek (1997). *Spikes: Exploring the neural code.* MIT Press.

Schöne, H. (1984). *Spatial orientation: The spatial control of behavior in animals and man.* Princeton University Press.

Schmidt-Koenig, K. and H. J. Schlichte (1972). Homing in pigeons with impaired vision. *Proc. Nat. Acad. Sci.* USA **69**:2446-2447.

Ward, S. (1973). Chemotaxis by the nematode *Caenorhabditis elegans*: Identification of attractants and analysis of the response by use of mutants. *Proc. Nat. Acad. Sci. USA* **70**:817-821.

White, J. G., E. Southgate, J. N. Thompson and S. Brenner (1986). The structure of the nervous system of *C. elegans. Phil. Trans. R. Soc. London* **314**:1-340.

Worst, R. and R. Linnemann (1996). Construction and operation of a snake-like robot. In *Proceedings of IEEE International Joint Symposia on Intelligence and Systems.* IEEE Computer Society Press.